Evolution of the momentum distribution with mass loss in projectile fragmentation reactions

K. Meierbachtol,[1,2] D. J. Morrissey,[1,2] M. Mosby,[1,2] and D. Bazin[2]
[1]*Department of Chemistry, Michigan State University, East Lansing, Michigan 48824, USA*
[2]*National Superconducting Cyclotron Laboratory, Michigan State University, East Lansing, Michigan 48824, USA*
(Received 20 December 2011; published 19 March 2012)

Background: Momentum distributions of fragmentation products as a function of fragment mass have been used to study the fragmentation mechanism. The parallel component of the momentum distribution has been well studied previously and modeled. The perpendicular component, however, is much less measured or understood.
Purpose: Measure both components of the linear momentum of a wide range of fragmentation products and compare the widths of the momentum distributions to previous results and descriptions.
Method: The parallel and perpendicular components of the momentum vector have been measured for projectile-like fragments produced in the reactions of ^{76}Ge with ^{9}Be and ^{197}Au at 130 MeV/nucleon in a magnetic spectrometer.
Results: The measured parallel momentum distributions of all fragments follow established systematics. The perpendicular momentum distributions of fragments produced by fragmentation by the ^{197}Au target with masses near that of the projectile exhibit a clear peak near the momentum corresponding to the grazing angle that diminishes with decreasing fragment mass.
Conclusions: The interplay between Coulomb and nuclear scattering can be used to describe results for the most peripheral collisions.

DOI: 10.1103/PhysRevC.85.034608 PACS number(s): 25.70.Mn, 25.60.Gc, 29.38.Db

I. INTRODUCTION

The study of fragments produced from fragmentation reactions has followed many paths with various observables used to probe the underlying reaction mechanism(s) involved. Measurements of the fragments' linear momentum distributions have been a key tool for examining the reaction mechanism. Distributions of either total momentum or its parallel (longitudinal) component have been measured for fragments produced from the interaction of a wide range of target and projectile combinations and projectile energies ranging from the Coulomb barrier to several GeV/nucleon [1–7]. This extensive library of measurements has led to a variety of empirical descriptions relating the momentum distributions to the produced fragment mass, and various conclusions regarding the contributing reaction mechanisms beyond pure fragmentation. The vast majority of these studies have deduced the presence of at least one additional component to the main fragmentation process. Although the parallel component of the momentum vector has been extensively measured and modeled, the much smaller, equally important, perpendicular component has not been as well studied. Characteristics of both components within the fragmentation mechanism are necessary to build a complete picture of the process.

Parallel momentum distribution measurements and descriptions of their widths are numerous. The early description of the distribution width by Goldhaber [1] only depends on the masses of the original projectile and the measured fragment and provides an excellent framework for describing the parallel momentum distributions. This simple description has been expanded as more results have been obtained [2,3,8,9].

The perpendicular (transverse) component of the momentum has been rarely measured, and its properties and role as an observable in the study of reaction mechanisms have not been tested. Unlike the parallel component which mostly reveals the amount of energy dissipated in the reaction, the perpendicular component is more sensitive to the reaction mechanism. The first measurement of the transverse momentum for projectile fragments by Van Bibber *et al.* used a ^{16}O beam at 90 and 120 MeV/nucleon [10]. The authors concluded that the width of the perpendicular momentum distribution can be described by adding a term to the parallel width given by Goldhaber that accounts for the orbital deflection of the projectile by the target during fragmentation. Subsequent measurements of the perpendicular momentum have involved only projectiles at high energies [11–14].

Precise measurements of outgoing fragments' positions and angles in a large acceptance spectrometer have made measuring the small perpendicular component much more feasible. Here we report measurements of the full momentum distributions of fragments produced by the reactions of a ^{76}Ge beam at 130 MeV/nucleon with ^{9}Be and ^{197}Au targets. The measurement of both the parallel and perpendicular components of the fragmentation residue momentum for a wide range of fragment species has made it possible to obtain a more comprehensive picture of these reactions.

II. EXPERIMENTAL METHOD

The experiment was performed at the National Superconducting Cyclotron Laboratory (NSCL) at Michigan State University. A ^{76}Ge primary beam was produced and accelerated to 130 MeV/nucleon at the Coupled Cyclotron Facility. The momentum spread of the beam was measured with the A1900 fragment separator [15] to be $<0.10\%$.

The ^{76}Ge beam was reacted with either of two targets, 99.8 mg/cm^2 ^{9}Be or 50.73 mg/cm^2 ^{197}Au, placed at the target position of the S800 spectrograph [16]. The forward-focused projectile-like fragments entered the large acceptance of the

 ©2012 American Physical Society

spectrograph and were dispersed on the focal plane detection system by the spectrograph's two dipole magnets. Fragment identification was performed using a combination of detectors in the focal plane. An ionization chamber measured each particle's energy loss [17], and the time-of-flight of each particle was measured as the time difference between two plastic scintillators located at the object position of the S800 beamline, and one downstream of the ionization chamber in the focal plane of the spectrograph. The residual energy signals from a newly installed CsI(Na) hodoscope [18] array were used to identify charge states of the fragments as part of the particle identification scheme and remove unwanted events from the analysis. This additional discrimination was required for events produced with the gold target only.

The full momentum vector was reconstructed on an event-by-event basis for a wide range of fragment species produced in the projectile fragmentation reaction. Position information from the cathode readout drift chambers (CRDCs) in the focal plane detection system was combined with trajectory reconstruction through the spectrograph using the COSY INFINITY code [19] to reconstruct both the longitudinal and transverse momentum distributions at the target position. To minimize error from events with trajectories near the physical limits of the spectrograph, the acceptance was limited to $\pm 4.07\%$ in momentum in the longitudinal direction and ± 52.2 mrad in the transverse direction. Several magnetic rigidity $B\rho$ settings of the S800 were used to collect the majority of the fragments produced in these reactions. The full parallel momentum distributions were reconstructed by combining the data obtained in each $B\rho$ setting. The contribution of the target thickness to the total width of the momentum distributions are only a few percent for fragments near the projectile and grow to 20% percent at the mass loss limit of this work. The perpendicular momentum distribution of each fragment was extracted from the $B\rho$ setting containing the peak of the fragment's parallel momentum distribution. This ensured a consistent evaluation, avoiding the possible effect of correlations between the two vector components. Examples of the distributions of the perpendicular momentum are shown in Fig. 1. Finally, each momentum distribution was transformed into the center-of-mass frame of the reaction, and the width σ of each Gaussian distribution was measured as well as the average parallel momentum transfer of each fragment.

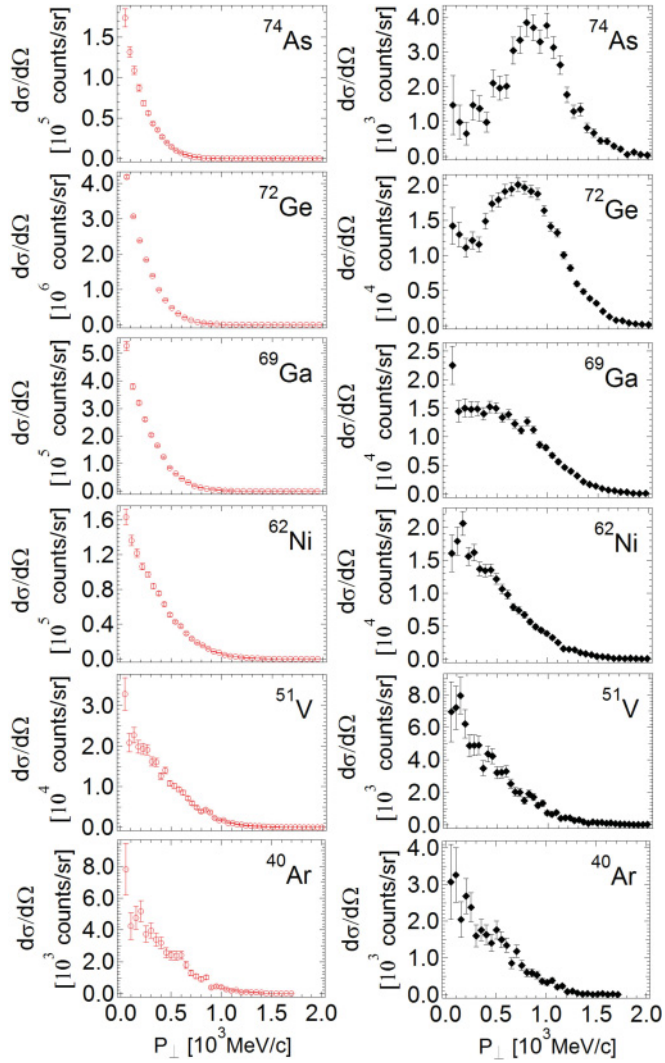

FIG. 1. (Color online) Measured perpendicular momentum distributions for six fragments produced from beryllium and gold targets (left and right columns, respectively): ^{74}As, ^{72}Ge, ^{69}Ga, ^{62}Ni, ^{51}V, and ^{40}Ar. Error bars shown are statistical only.

III. RESULTS AND DISCUSSION

A. Parallel momentum distributions

The width of each fragment's parallel distribution is presented in Fig. 2 as a function of the observed change in mass number ΔA, where $\Delta A = A_{\text{projectile}} - A_{\text{fragment}}$, from the projectile ^{76}Ge, for fragments produced from interaction with both the ^{9}Be and ^{197}Au targets. The data clearly indicate that there is no significant difference between the two targets. The two data sets overlap so well that the 70 isotopes that were observed in both cases cannot be distinguished by parallel distribution values alone. The measured distributions of the parallel component of the momentum vector for the fragments agree well with previously published results [2–6,10,20,21] and fill a gap in the data for medium mass species and intermediate projectile energy. This result strongly supports previous models' exclusion of any target parameters in their descriptions of the parallel distribution widths.

Two empirical models have been fitted to the data. The first was produced by Goldhaber [1]:

$$\sigma_{p_\parallel}^2 = \sigma_o^2 \frac{K(A-K)}{A-1}, \tag{1}$$

where K is the fragment mass, A is the projectile mass, and the coefficient σ_0, also called the reduced width, is estimated by the total Fermi momentum p_F of the uncorrelated nucleons in the projectile as

$$\sigma_o = \frac{p_F}{\sqrt{5}}. \tag{2}$$

The value of p_F can be determined from electron scattering measurements on the nucleus of interest. The second model

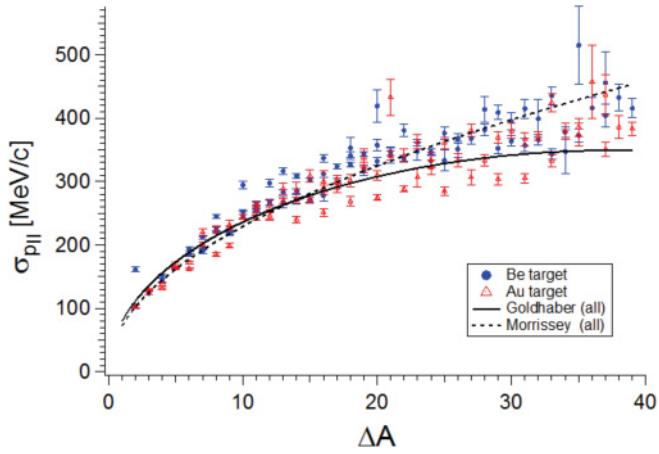

FIG. 2. (Color online) Widths of parallel momentum component distributions are shown as a function of mass loss (ΔA) for two target species, beryllium (circles) and gold (triangles). Solid and dashed lines represent the best fits to the data for the Goldhaber and Morrissey models, respectively.

was produced by Morrissey [8]:

$$\sigma_{p_\parallel}^2 = \sigma_o^2 \sqrt{\Delta A}, \tag{3}$$

where $\Delta A = A_{\text{projectile}} - A_{\text{fragment}}$ and σ_o^2 is a constant determined from data. Both models include a simple dependence on the mass loss (ΔA) associated with each fragment, while Goldhaber also includes the mass of the projectile. The fitted functions both follow the data with no clear "best" model between the two based on overlapping reduced χ^2 values. The experimental value of the coefficient σ_1 determined for both models with the complete data set are compared to other experimental values in Table I. The coefficient values obtained from best fits to the data are smaller than Goldhaber and Morrissey's original coefficients but still consistent with other published values [1–6] except that at lowest energy [5] there is not a simple energy dependence of the data from the literature. The original model by Goldhaber calculated σ_1 from the Fermi momentum of the projectile. The σ_1 value reported here was treated as an independent fitting parameter similar to past applications of this model and is 30% smaller than that predicted using the Fermi momentum from Moinz [22].

It should be noted that a few fragments with one more proton than the beam were also observed in this work. The widths of these fragment parallel distributions are included in Fig. 2 results as well as in the fit to the data with both models. While these fragments are not produced by pure fragmentation, the widths of their parallel momentum distributions are in agreement with the empirical fragmentation models' predictions. An analysis of the parallel momentum widths for isobaric chains indicated there is no dependence on atomic number Z.

The parallel downshift or momentum transfer associated with each fragment was also measured and compared to previous results [6]. The mean parallel momentum transfer shown in Fig. 3 as $-\langle P_\parallel \rangle$ was defined as the loss in momentum between the projectile momentum and the fragment's final average measured momentum. The dashed lines on both plots are the best linear fits to the two data sets. The slope parameters of these fits are 6.2 and 4.8 MeV/c for the beryllium and gold target plots, respectively. These values are smaller than the linear relationships of 8.0 and 8.8 MeV/c reported by Morrissey [8] and Pfaff [6] but still follow the same linear trend; and for the beryllium data set, a leveling off of momentum transfer for larger mass loss values matches the results seen by Morrissey. Isotope chains $Z = 33$ through $Z = 27$ also exhibit fairly constant and steeper slopes than the average, with the beryllium target species having even larger slope values than the gold target species. This increase in the slope parameter values for fragments near the projectile Z value agrees with trends seen by Pfaff [6]. However, fragments with one more proton than the projectile species of ^{76}Ge do not have slope parameters deviating significantly from slopes for fragments with atomic numbers at or below the projectile species, a disagreement with that seen by Pfaff [6].

B. Perpendicular momentum distributions

The high angular acceptance and resolution of the S800 spectrometer enabled the measurement of the much smaller perpendicular momentum distributions over a wide mass range of projectile-like fragments produced from the ^{76}Ge beam on both ^{9}Be and ^{197}Au targets. The widths extracted for the perpendicular momentum distributions of fragments produced from the ^{9}Be target as well as those for fragments with

TABLE I. Coefficient values in units of MeV/c resulting from application of Goldhaber (G) and Morrissey (M) models to a variety of data sets in the literature. Multiple coefficient values correspond to the multiple target or energies of the corresponding reaction.

Ref.	Reaction	Energy/nucleon	σ_0(G)	σ_0(M)
[1]	^{16}O + Be	2.1 GeV	90	
[2]	^{12}C,^{16}O + Be-Pb	1.05,2.1 GeV	71,86	
[3]	Data from [2]	Data from [2]	103,104	
[4]	^{40}Ar + ^{68}Zn	27.6 MeV	109	
[5]	^{40}Ar + ^{40}Ca	27,44 MeV	95,85	
[5]	^{20}Ne + ^{208}Pb	44 MeV	45	
[6]	^{86}Kr + ^{27}Al	70 MeV	124	120
[8]	Data from [2]	Data from [2]		94
This work	^{76}Ge + ^{9}Be,^{197}Au	130 MeV	80	73

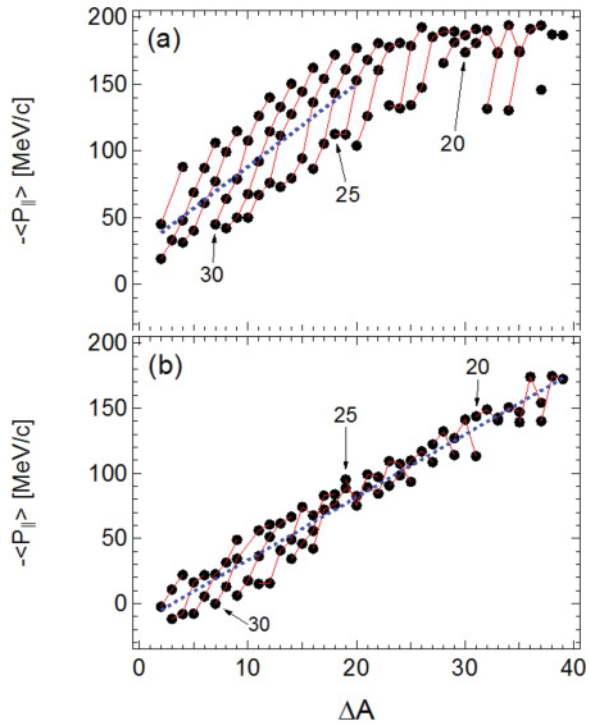

FIG. 3. (Color online) Momentum transfer vs mass loss (ΔA) for fragments produced using beryllium (a) and gold (b) targets. The dashed lines show the best linear fits to the data and correspond to slopes of 6.2 and 4.8 MeV/c for beryllium and gold target data sets. The solid lines connect isotopes with $Z = 33$ to $Z = 17$. The numbers on the plot indicate isotope chains $Z = 30$, 25, and 20. The uncertainties in the data are smaller than the symbols.

mass $\leqslant 69$ produced from the ^{197}Au target that were found to be peaked at zero momentum (0° in scattering angle) are shown in Fig. 4. Width results for fragments near the projectile mass ($\geqslant$70) from the ^{197}Au target were not peaked at zero momentum and are discussed separately below.

The widths of the perpendicular momentum distributions presented in Fig. 4 were compared to the empirical description by Van Bibber *et al.* that adds a term to the definition of parallel width by Goldhaber [1] to include a contribution from the orbital deflection of the projectile by the target in addition to the intrinsic nucleon motion of the fragment that generates the longitudinal width [10]:

$$\sigma_{p_\perp}^2 = \sigma_o^2 \frac{F(A-F)}{A-1} + \sigma_1^2 \frac{F(F-1)}{A(A-1)}, \tag{4}$$

where A = projectile mass, F = fragment mass, and σ_1 is the variance of the transverse momentum of the projectile

$$\sigma_1^2 = \tfrac{1}{2}\langle p_\perp^2 \rangle. \tag{5}$$

The Morrissey definition of the parallel width term [8] was also applied to the perpendicular widths from the beryllium target fragments by combining Morrissey's term and Van Bibber's second term. As is shown in Fig. 4 these empirical

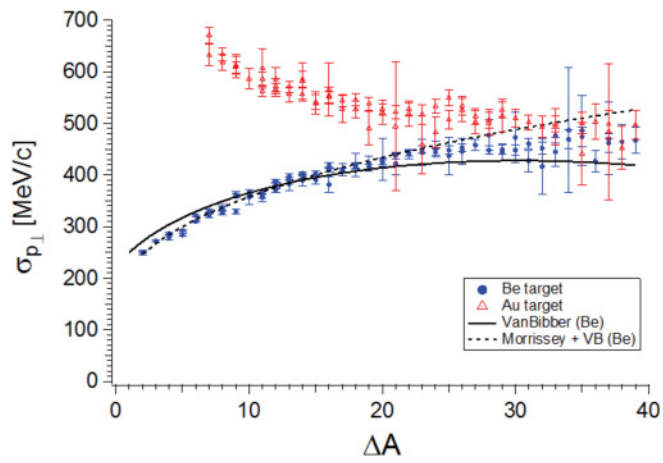

FIG. 4. (Color online) Widths of distribution of perpendicular momentum component as a function of mass loss (ΔA) for two target species, beryllium (circles) and gold (triangles). Solid and dashed lines show the best fits to the data using models from Van Bibber and Morrissey plus Van Bibber's orbital deflection term, respectively, for the beryllium target data only.

descriptions correctly describe all the fragments produced from the beryllium target and fragments with $\Delta A \geqslant 20$ for the gold target, regardless of which description of the parallel component was used. The assumption that the parallel distribution widths determine the σ_0 coefficient was also tested by (1) fixing the σ_0 coefficient to values obtained from the parallel distribution widths alone and (2) allowing the σ_0 coefficient to remain as a free parameter. As can be seen in Table II both approaches resulted in similar values for the coefficients.

This description of the widths from Van Bibber *et al.* assumes scattering of the fragments uniformly around the perimeter of the target nucleus, which in turn implies that the perpendicular momentum distribution should be peaked at zero momentum. The fragments with $\Delta A < 20$ from the gold target clearly diverge from this simple model, see Fig. 1, and the measured perpendicular distributions for those fragments with $70 \leqslant A \leqslant 74$ have a peak just below the momentum value corresponding to the grazing angle. The observed peak shifts systematically to zero as the fragment mass decreases, and

TABLE II. Coefficient values σ_0 and σ_1 in units of MeV/c resulting from application of models from Van Bibber and Morrissey + Van Bibber's second term (Morrissey + VB). Fixed σ_0 coefficient values were obtained after fixing the σ_0 coefficient value to the values obtained in parallel distribution width fitting process. Free σ_0 values were obtained after allowing both coefficients to be free parameters in the fitting process.

	Fixed σ_0		Free σ_0	
Ref.	σ_0	σ_1	σ_0	σ_1
Van Bibber	80 ± 1	140 ± 1	86 ± 1	125 ± 1
Morrissey + VB	73 ± 1	146 ± 1	70 ± 1	155 ± 1

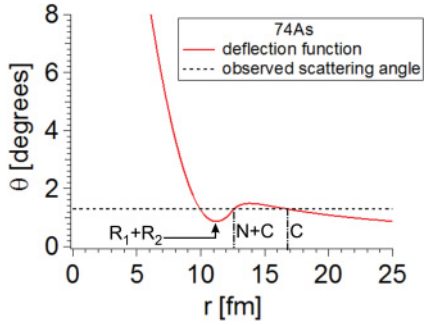

FIG. 5. (Color online) Calculated deflection angle as a function of impact parameter for ^{74}As. The dashed line is the observed peak scattering angle for this fragment. The sum of the two nuclear radii, $R_1 + R_2$, from the definition in Ref. [23] is indicated by the arrow. The N + C and C labels refer to impact parameters associated with nuclear plus Coulomb and pure Coulomb scattering (see text).

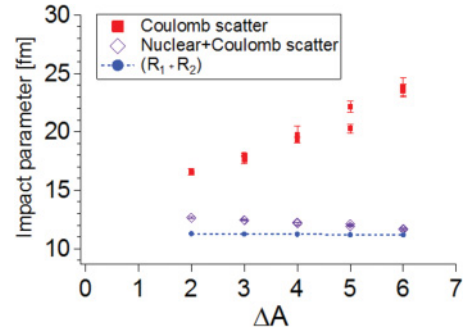

FIG. 6. (Color online) Calculated impact parameters associated with measured scattering angles for the heaviest fragments from a gold target as a function of projectile mass loss, ΔA, see the text.

then the width of the distribution decreases toward the values found for the ^{9}Be target.

These results are a clear deviation from the empirical prediction by Van Bibber *et al*. of perpendicular momentum distributions for fragmentation species and indicate that a better description of the scattering process is needed. The interplay of the Coulomb and nuclear potentials that leads to this behavior can be explored with a simple calculation of the classical deflection angle as a function of impact parameter [24]. Figure 5 shows an example of such a calculation for ^{74}As, with $\Delta A = 2$ from ^{76}Ge. The interaction potential was taken to be the sum of the Coulomb potential and the nuclear proximity potential [23]. This calculation includes the assumption of a single trajectory for the projectile with no higher order terms, such as energy dissipation, taken into consideration. The nuclear potential, approximated by the proximity potential, treats the two nuclei as gently curved slabs separated by a small gap and an attractive force determined by parameters for the average radius of the two nuclei. The resulting deflection angles were compared to the measured peak scattering angle for fragments with $\Delta A < 7$. As can be seen in Fig. 5, the observed scattering angle corresponds in the deflection function to two impact parameters that are larger than the sum of the two nuclear radii, $R_1 + R_2$, as defined in Ref. [23]. The larger of the two calculated impact parameters corresponds to a scattering angle due to the Coulomb (C) potential alone, while the smaller impact parameter corresponds to scattering due to the nuclear plus Coulomb (N + C) potentials.

The two impact parameters that correspond to the observed peak scattering angle are shown in Fig. 6 as a function of the number of removed nucleons from the projectile. These impact parameters indicate that the data are clearly inconsistent with Coulomb scattering alone as the source of the measured scattering angles for fragments with masses of $\Delta A < 7$. The impact parameter values associated with Coulomb scattering have a large separation between the projectile and target which would preclude the necessary overlap of nuclear density for producing the observed fragment species. On the other hand, the calculated impact parameter which comes from the nuclear plus Coulomb scattering scenario decreases slightly with increasing mass loss and approaches the sum of the radii. This evolution follows the measured trend of decreasing scattering angle. The measured peak scattering angle for fragments above $\Delta A = 7$ becomes essentially zero, and the width of the distribution decreases toward the limiting value seen in the Van Bibber expression.

IV. SUMMARY

The full momentum distributions of fragmentation products produced by heavy ion reactions at intermediate energies have been measured. Both the parallel and perpendicular components of the fragment momentum vector were measured for a wide range of fragment masses from a ^{76}Ge beam, and the properties of the distributions were obtained as a function of fragment mass loss. The parallel momentum transfer of the fragments was found to have a linear dependence on fragment mass loss similar to earlier work. The widths of all of the fragment parallel momentum distributions were found to follow established empirical descriptions and were independent of target. The widths of the perpendicular momentum distributions, however, cannot be described by fragment mass alone. The perpendicular widths of the heaviest products clearly show deflection by the gold target. All fragments produced from a light target and fragments produced from a heavy target with $\Delta A \geqslant 20$ follow previously published descriptions of the perpendicular width as a function of fragment mass. The fragments from a heavy target with a small mass loss were found to be consistent with the predictions from a qualitative classical calculation of the deflection angle as a function of impact parameter. The calculated impact parameter at the peak scattering angle from the combined effect of nuclear and Coulomb potentials was found to be very close to the sum of the nuclear radii. The present data provide a test for more detailed theoretical calculations of the fragmentation process.

ACKNOWLEDGMENTS

This work was supported by the National Science Foundation under Grants No. PHY-06-06007 and No. PHY-11-02511.

[1] A. S. Goldhaber, Phys. Lett. B **53**, 306 (1974).
[2] D. E. Greiner, P. J. Lindstrom, H. H. Heckman, B. Cork, and F. S. Bieser, Phys. Rev. Lett. **35**, 152 (1975).
[3] W. A. Friedman, Phys. Rev. C **27**, 569 (1983).
[4] F. Rami, J. P. Coffin, G. Guillaume, B. Heusch, P. Wagner, A. Fahli, and P. Fintz, Z. Phys. A **318**, 239 (1984).
[5] Y. Blumenfeld, PH. Chomaz, N. Frascaria, J. P. Garron, J. C. Jacmart, J. C. Roynette, D. Ardouin, and W. Mittig, Nucl. Phys. A **455**, 357 (1986).
[6] R. Pfaff, D. J. Morrissey, M. Fauerbach, M. Hellström, J. H. Kelley, R. A. Kryger, B. M. Sherrill, M. Steiner, J. S. Winfield, J. A. Winger, S. J. Yennello, and B. M. Young, Phys. Rev. C **51**, 1348 (1995).
[7] E. Hanelt, A. Grewe, K.-H. Schmidt, T. Brohm, H.-G. Clerc, M. Dornik, M. Fauerbach, H. Geissel, A. Magel, G. Münzenberg, F. Nickel, M. Pfützner, C. Scheidenberger, M. Steiner, K. Sümmerer, B. Voss, M. Weber, J. Weckenmann, and C. Ziegler, Z. Phys. A **346**, 43 (1993).
[8] D. J. Morrissey, Phys. Rev. C **39**, 460 (1989).
[9] C.A. Bertulani and K.W. McVoy, Phys. Rev. C **46**, 2638 (1992).
[10] K. Van Bibber, D. L. Hendrie, D. K. Scott, H. H. Weiman, L. S. Schroeder, J. V. Geaga, S. A. Cessin, R. Treuhaft, Y. J. Grossiord, J. O. Rasmussen, and C. Y. Wong, Phys. Rev. Lett. **43**, 840 (1979).
[11] J. Dreute, W. Heinrich, G. Rusch, and B. Wiegel, Phys. Rev. C **44**, 1057 (1991).
[12] F. P. Brady, W. B. Christie, J. L. Romero, C. E. Tull, J. L. Chance, G. P. Grim, J. C. Young, H. J. Crawford, T. Kobayashi, P. J. Lindstrom, D. L. Olson, T. J. M. Symons, I. Tanihata, H. Wieman, W. F. J. Müller, H. Sann, and U. Lynen, Phys. Rev. C **50**, R525 (1994).
[13] J. L. Chance *et al*., Phys. Rev. C **64**, 014610 (2001).
[14] G. Hüntrup, T. Streibel, and W. Heinrich, Phys. Rev. C **65**, 014605 (2001).
[15] D. J. Morrissey, B. M. Sherrill, M. Steiner, A. Stolz, and I. Wiedenhöever, Nucl. Instrum. Methods Phys. Res., Sect. B **204**, 90 (2003).
[16] D. Bazin, J.A. Caggiano, B.M. Sherrill, J. Yurkon, and A. Zeller, Nucl. Instrum. Methods Phys. Res., Sect. B **20**, 629 (2003).
[17] J. Yurkon, D. Bazin, W. Benenson, D. J. Morrissey, B. M. Sherrill, D. Swan, and R. Swanson, Nucl. Instrum. Methods Phys. Res., Sect. A **422**, 291 (1999).
[18] K. Meierbachtol, D. Bazin, and D. J. Morrissey, Nucl. Instrum. Methods Phys. Res., Sect. A **652**, 668 (2011).
[19] K. Makino and M. Berz, Nucl. Instrum. Methods Phys. Res., Sect. A **427**, 338 (1999).
[20] M. Weber *et al*., Nucl. Phys. A **578**, 659 (1994).
[21] J. Reinhold, J. Friese, H.-J. Körner, R. Schneider, K. Zeitelhack, H. Geissel, A. Magel, G. Münzenberg, and K. Sümmerer, Phys. Rev. C **58**, 247 (1998).
[22] E. J. Moinz, I. Sick, R. R. Whitney, J. R. Ficenec, R. D. Kephart, and W. P. Trower, Phys. Rev. Lett. **26**, 445 (1971).
[23] J. Blocki, J. Randrup, W. J. Światecki, and C. F. Tsang, Ann. Phys. (NY) **105**, 427 (1977).
[24] C. A. Bertulani and P. Danielewicz, *Introduction to Nuclear Reactions* (Institute of Physics, London, 2004).